Charge ordering in reactive sputtered (1 0 0) and (1 1 1) oriented epitaxial Fe3O4 films

ARTICLE *in* SCRIPTA MATERIALIA · JUNE 2013

Impact Factor: 3.22 · DOI: 10.1016/j.scriptamat.2013.02.050

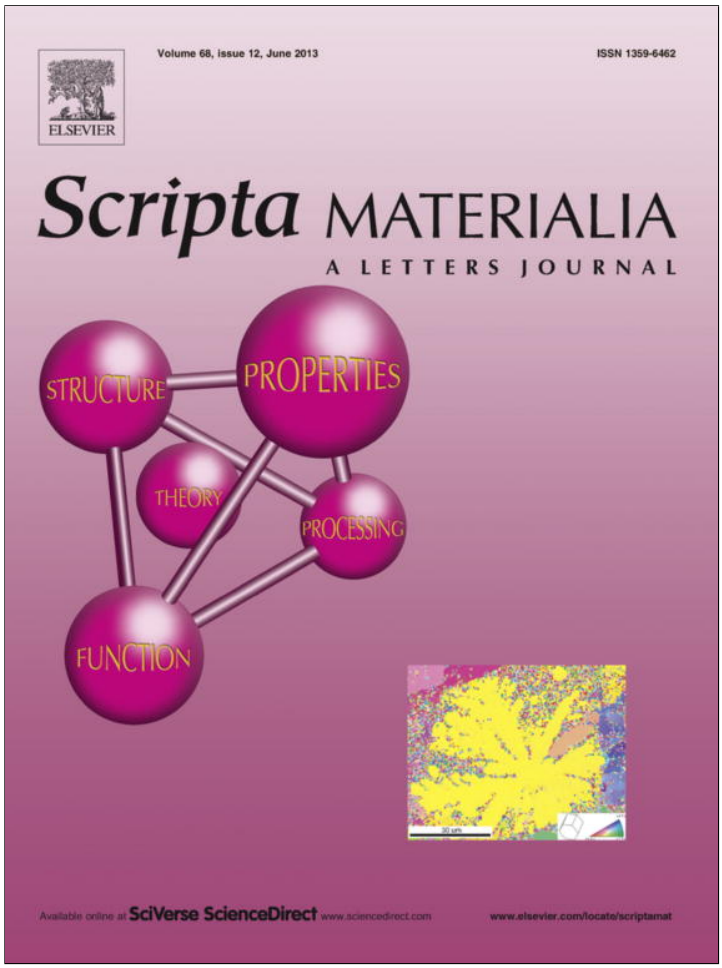

Available online at www.sciencedirect.com

SciVerse ScienceDirect

Scripta Materialia 68 (2013) 972–975

Scripta MATERIALIA

www.elsevier.com/locate/scriptamat

Charge ordering in reactive sputtered (100) and (111) oriented epitaxial Fe_3O_4 films

Wenbo Mi,[a,*] Zaibing Guo,[b] Qingxiao Wang,[b] Yang Yang[b] and Haili Bai[a]

[a]*Tianjin Key Laboratory of Low Dimensional Materials Physics and Preparation Technology, Institute of Advanced Materials Physics, Faculty of Science, Tianjin University, Tianjin 300072, People's Republic of China*
[b]*Core Labs, King Abdullah University of Science and Technology (KAUST), Thuwal 23955-6900, Saudi Arabia*

Received 19 February 2013; accepted 25 February 2013
Available online 5 March 2013

Epitaxial Fe_3O_4 films with (100) and (111) orientations fabricated by reactive sputtering present simultaneous magnetic and electrical transitions at 120 and 124 K, respectively. The symmetry decreases from face-centered cubic to monoclinic structure across the Verwey transition. Extra spots with different brightness at different positions appear in selected-area diffraction patterns at 95 K. The extra spots come from the charge ordering of outer-layer electrons of Fe atoms, and should be related to the charge ordering of octahedral B-site Fe atoms.

Keywords: Fe_3O_4/magnetite; Charge ordering; Raman spectrum; Selected-area diffraction patterns

Fe_3O_4 undergoes a metal–insulator transition near 120 K, which is the so-called Verwey transition [1]. Verwey et al. proposed that this transition should be correlated with the formation of the charge ordering of the Fe^{2+} and Fe^{3+} ions on the octahedral sites of the inverse spinel structure of Fe_3O_4 [2]. At the Verwey temperature (T_V), Fe_3O_4 undergoes a transition from a cubic structure with lattice constants of $a = b = c =$ 0.839 nm to a monoclinic form with lattice constants of $a = 0.5944$ nm, $b = 0.5925$ nm, $c = 1.6775$ nm and $\beta = 90.2365°$ [3]. At T_V, changes in latent heat [4] and a two-order-of-magnitude decrease in DC conductivity [5] have also been observed. The Verwey model assumes a purely electronic mechanism of the Verwey transition, leading to an ordering of Fe^{2+} and Fe^{3+} ions in the B chain, along the [110] and [1$\bar{1}$0] directions below T_V, respectively. Anderson suggested that the charge ordering in the form of a charge density wave is stabilized by interionic electrostatic energy, where each B tetrahedron consists of two Fe^{2+} and two Fe^{3+} ions [6]. Anderson's long-range order–short-range order model was studied in a Hubbard-like model with interatomic d–d Coulomb interactions [7], However, it has not been confirmed by nuclear magnetic resonance and Mössbauer measurements [8]. There are some other theories explaining the Verwey transition, including charge-orbital ordering within the oxygen 2p states [9], a cooperative Jahn–Teller effect [10], Cullen and Callen's theory based on pure electron correlations [11], and a polaron-based theory of the transition [12,13]. The microscopic mechanism of the Verwey transition remains controversial. Recently, the structure of Fe_3O_4 was investigated using synchrotron X-ray powder diffraction above and below T_V [14,15]. The "trimerons" model was proposed by Senn et al. [15]. However, electron diffraction is the most effective method to observe the charge ordering. So far, only Rudee et al. have observed extra spots at room temperature in the epitaxial Fe_3O_4 film [16]. In this paper, epitaxial Fe_3O_4 films were fabricated using reactive sputtering. The T_V of the (100) oriented film is 120 K, and that of the (111) oriented one is 124 K. The first-order transition from cubic to monoclinic structure can be observed in Raman spectra measured at different temperatures. The extra spots in the electron diffraction patterns at 95 K indicate the charge ordering below T_V. According to the brightness and distribution of the extra spots, the charge ordering should be related to the "trimerons" model of the octahedral sites (B sites).

Epitaxial Fe_3O_4 films were fabricated on MgO(100) and Al_2O_3(0001) substrates using a DC magnetron sputtering apparatus from a pure Fe (99.99%) target. When the base pressure reached 6.0×10^{-8} Torr, an

* Corresponding author. Tel.: +86 22 27406991; fax: +86 22 27403425; e-mail: miwenbo@tju.edu.cn

1359-6462/$ - see front matter
http://dx.doi.org/10.1016/j.scriptamat.2013.02.050

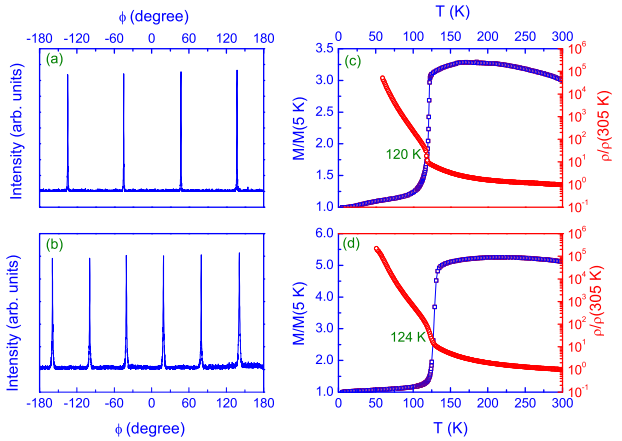

Figure 1. X-ray φ scan of the Fe_3O_4 films on (a) MgO(100) and (b) Al_2O_3(0001). The M–T and ρ–T curves of the Fe_3O_4 film on (c) MgO(100) and (d) Al_2O_3(0001) substrates.

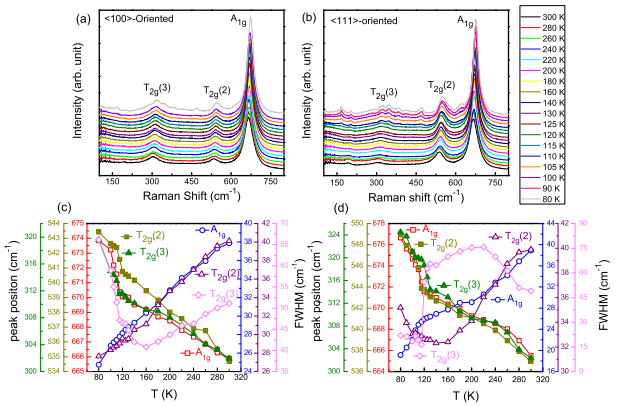

Figure 2. Raman spectra of the Fe_3O_4 films on (a) MgO(100) and (b) Al_2O_3(0001) substrates measured at different temperatures. Temperature-dependent peak position and full width at half maximum (FWHM) of the different Raman peaks of the Fe_3O_4 films on (c) MgO(100) and (d) Al_2O_3(0001) substrates.

Ar (99.999%) and O_2 (99.999%) gas mixture was introduced into the chamber to a pressure of 8 mTorr with a mixing ratio of Ar:O_2 = 50:3.5. The sputtering power was fixed at 150 W. The substrate temperature was kept at 700 °C during the film growth. The film thickness was about 200 nm determined using a Dektak 6M surface profiler and confirmed by transition electron microscopy (TEM). The structure of the films was characterized using X-ray diffraction φ scan and high-resolution TEM. The samples for TEM observation were prepared using focused ion beam etching. A Quantum Design physical property measurement system was used to measure the electrical transport properties of the films at temperatures ranging from 2 to 300 K. The magnetic properties were measured using a Quantum Design SQUID.

Figure 1a and b show the X-ray φ scan of the Fe_3O_4 films on MgO(100) and Al_2O_3(0001) substrates, respectively. For the film on MgO(100) substrate, φ scans were performed at $\alpha = 35.3°$ and the diffraction from the (111) plane was collected. Four peaks were observed, indicating the Fe_3O_4 film is epitaxial with(100) orientation. For the film on Al_2O_3(0001) substrate, φ scans were also performed at $\alpha = 35.3°$ and the diffraction from the (400) plane was collected. Six peaks were observed, which indicates the Fe_3O_4 film is epitaxial, but with (111) orientation. Figure 1c and d give the M–T and ρ–T curves of the epitaxial Fe_3O_4(100) and (111) films, respectively. Both the M–T and ρ–T curves show a sharp transition around 120 K. However, the T_V of the epitaxial Fe_3O_4(100) film on MgO(100) substrate is 120 K, smaller than $T_V \approx 124$ K of Fe_3O_4(111) film on Al_2O_3 substrate. This phenomenon may be due to the fact that the antiphase boundary density in Fe_3O_4(100) films is larger than that in Fe_3O_4(111) films [17].

Above T_V, Fe_3O_4 has a cubic-inverse-spinel structure belonging to the space group O_h^7 ($Fd3m$). The full unit cell contains 56 atoms but the smallest Bravais cell contains 14 atoms [18]. As a result, there should be 42 vibrational modes. Group theory has predicted the modes of $A_{1g} + E_g + T_{1g} + 3T_{2g} + 2A_{2u} + 2E_{2u} + 5T_{1u} + 2T_{2u}$ [18],

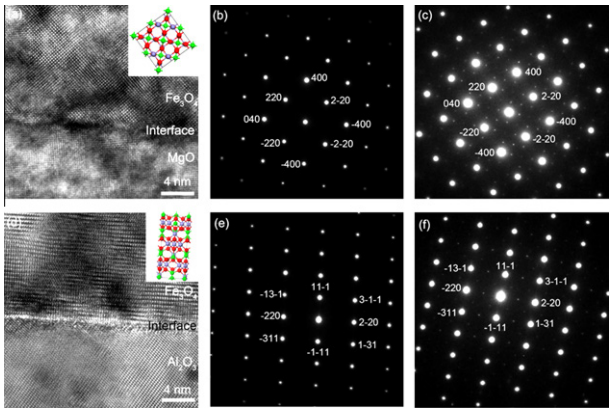

Figure 3. High-resolution TEM image of the Fe_3O_4 film on (a) MgO(100) and (d) Al_2O_3(0001) substrates. The room-temperature selected-area diffraction (SAED) patterns of the Fe_3O_4 film on (b) MgO(100) and (e) Al_2O_3(0001). The SAED patterns at 95 K of the Fe_3O_4 film on (c) MgO(100) and (f) Al_2O_3(0001).

but the T_{1g}, A_{2u}, E_u and T_{2u} are silent. Thus, there are five Raman-active modes ($A_{1g} + E_g + 3T_{2g}$) and five infrared active modes ($5T_{1u}$) [18]. Below T_V, the unit cell contains 56 atoms. The expected 168 modes predicted by group theory are the following modes $23A_g + 18A_u + 24B_{1g} + 19B_{1u} + 16B_{2g} + 27B_{2u} + 15B_{3g} + 26B_{3u}$ [18,19]. However, the A_u modes are silent. Thus, there are 78 Raman-active modes ($23A_g + 24B_{1g} + 16B_{2g} + 15B_{3g}$) and 72 infrared active modes ($19B_{1u} + 27B_{2u} + 26B_{3u}$) [18]. A dramatic increase in the number of Raman modes will appear in the low-temperature phase [18]. In order to investigate the transition from cubic to monoclinic, Raman spectra were recorded at different temperatures from 80 to 300 K, as shown in Figure 2. In Figure 2a and b, peaks located at 195, 304, 538 and 667 cm^{-1} can be observed above T_V, which are T_{2g}^1, T_{2g}^3, T_{2g}^2 and A_{1g}, respectively. However, below T_V, 11 peaks can be observed, which are located at 167, 200, 322, 346, 364, 385, 415, 471, 550, 619 and 676 cm^{-1}. The increased number of Raman modes should be attributed to the reduced symmetry, implying that the

transition occurs at T_V [18,19]. Figure 2c and d give the temperature-dependent peak position and full width at half maximum (FWHM) of T_{2g}^3, T_{2g}^2 and A_{1g} Raman peaks of the epitaxial Fe_3O_4 films with different orientations. A significant decrease of the Raman peak positions is observed around T_V, as observed by Gupta et al. [20] and Phase et al. [21]. In Figure 2c, the line width of T_{2g}^2 and A_{1g} for the (100) film linearly increases with the increased temperature, which is attributed to the thermal effect. The temperature dependence of T_{2g}^2 line width is similar to that reported by Gupta et al. [20], but that of A_{1g} is different from that noted by Gupta et al. [20] and Phase et al. [21]. The line width of T_{2g}^3 shows a sudden decrease around T_V, consistent with that reported by Gupta et al. [20] and Phase et al. [21]. However, the value of the T_{2g}^3 line width is smaller than that observed by Gupta et al. [20], but larger than that observed by Phase et al. [20]. In Figure 2d, the line width of the T_{2g}^3 and A_{1g} modes for the (111) oriented film shows a significant increase around T_V, but no significant change can be observed for T_{2g}^3 line width at T_V, which is different to the (100) oriented film.

It is very interesting that the extra spots from the superlattices can be observed from the selected-area electron diffraction (SAED) patterns below T_V due to the ordering of the outer electrons. Electron diffraction provides sufficient sensitivity to probe the charge ordering [16,22]. Figure 3a and d show the cross-sectional HRTEM images of the Fe_3O_4/MgO and Fe_3O_4/Al_2O_3 interfaces, respectively. The reactive sputtered Fe_3O_4 layers grow epitaxially on the MgO and Al_2O_3 substrates with a sharp interface. Figure 3b and e show the SAED spots at room temperature from the Fe_3O_4 layers on MgO and Al_2O_3 substrates, respectively. Figure 3c and f show the SAED patterns at 95 K. The presence of extra spots between the spots of those appearing at room temperature is very obvious, suggesting that charge ordering exists below T_V. However, the extra spot at the midpoint of four regular spots in the <100> orientation was weaker than its neighbors. In addition, the extra spot at the midpoint of (220) orientation is also weaker than others, but the one at the midpoint of the $(2\bar{2}0)$ orientation is the same as the others. The change in the brightness is observed in the Fe_3O_4 layers with different orientations.

It is well known that if the extra diffraction spots are from the charge ordering of B-site Fe atoms that follows the Verwey model, the brightness of the extra diffraction spots at the midpoint of (220) and $(2\bar{2}0)$ orientation should be same. Meanwhile, the brightness of the extra spots in the <100> orientation should be stronger rather than weaker. Therefore, the extra diffraction spots probably do not come from the charge ordering of B-site Fe^{2+} and Fe^{3+} ions. On the other hand, the intensity of the extra spots should also be same if they are from the O-atom sites. From the above analyses, the extra spots may be from the A-site Fe atoms. Rudee et al. also observed similar SAED spots with different brightness in (100) epitaxial Fe_3O_4 films on MgO(100) substrate [16], observing that a structural model that included one vacancy on a tetrahedral site in every fifth unit cell produced a remarkably good fit by simulating the diffraction pattern using MacTempas software for the observed diffraction patterns [16]. However, it is well known that there are only Fe^{3+} ions on the tetrahedral sites, and no charge ordering should appear. Meanwhile, below T_V, the lattice displacements should appear [3], which may also affect the SAED patterns. The lattice displacements associated with the Verwey transition in Fe_3O_4 have been detected by neutron diffraction [3]. However, the displacement is only a few per cent, which cannot produce such obvious extra spots. Recently, the structure of Fe_3O_4 was investigated using synchrotron X-ray powder diffraction above and below T_V [14,15]. The "trimerons" model was proposed by Senn et al. [15]. Based on the "trimerons" model shown in Figure 4d in Ref. [15], the extra spots in our SAED pattern should appear, and the brightness of the extra spots should be different because the number of atoms those contribute to the different extra spots is different, which is consistent with our SAED results. Therefore, one can conclude that the extra spots should be related with the charge ordering of the octahedral B-site Fe atoms according to the "trimerons" model.

In summary, the Verwey transition in epitaxial Fe_3O_4 films has been observed in magnetic and electrical measurements around 120 K with the decrease in the symmetry from face-centered cubic to monoclinic structure. It is highly significant that the extra spots from the superlattice structure with different brightness at different positions have been observed in the SAED patterns at 95 K. Based on the distribution and brightness of the extra spots, the appearance of the extra spots should be related to the charge ordering of the octahedral B-site Fe atoms according to the "trimerons" model.

This work was supported by the National Natural Foundation of China (51172126) and the Key Project of Natural Foundation of Tianjin City (12JCZDJC27100).

[1] E.J.W. Verwey, P.W. Haayman, Physica (Utrecht) 8 (1941) 979.
[2] E.J.W. Verwey, P.W. Haayman, F.C. Romeijan, J. Chem. Phys. 15 (1947) 181.
[3] M. Iizumi, T.F. Koetzle, G. Shirane, S. Chikazumi, M. Matsui, S. Todo, Acta Crystallogr. B 38 (1982) 2121.
[4] J.P. Shepherd, J.W. Koenitzer, R. Aragón, C.J. Sandberg, J.M. Honig, Phys. Rev. B 31 (1985) 1107.
[5] T. Fujii, M. Takano, R. Katano, Y. Bando, Y. Isozumi, J. Appl. Phys. 7 (1989) 3168.
[6] P.W. Anderson, Phys. Rev. 102 (1956) 1008.
[7] J.R. Cullen, E. Callen, J. Appl. Phys. 41 (1970) 879.
[8] J. Garcia, G. Subias, J. Phys. Condens. Matter 16 (2004) R145.
[9] D.J. Huang, H.J. Lin, J. Okamoto, K.S. Chao, H.T. Jeng, G.Y. Guo, C.H. Hsu, C.M. Huang, D.C. Ling, W.B. Wu, C.S. Yang, C.T. Chen, Phys. Rev. Lett. 96 (2006) 096401.
[10] D. Schrupp, M. Sing, M. Tsunekawa, H. Fujiwara, S. Kasai, A. Sekiyama, S. Suga, T. Muro, V.A.M. Brabers, R. Claessen, Europhys. Lett. 70 (2005) 789.
[11] J.R. Cullen, E.R. Callen, J. Appl. Phys. 41 (1970) 879.
[12] N.F. Mott, Philos. Mag. B 42 (1980) 327.
[13] I.G. Austin, N.F. Mott, Adv. Phys. 18 (1969) 41.

[14] J. Blasco, J. Garcia, G. Subias, Phys. Rev. B 83 (2011) 104105.
[15] M.S. Senn, J.P. Wright, J.P. Attfield, Nature 481 (2012) 173.
[16] M.L. Rudee, D.J. Smith, D.T. Margulies, Phys. Rev. B 59 (1999) R11633.
[17] S.M. Thompson, V.K. Lazarov, R.C. Bradley, T. Deakin, B. Kaeswurm, G.E. Sterbinsky, J. Cheng, B.W. Wessels, J. Appl. Phys. 107 (2010) 09B102.
[18] L.V. Gasparov, D.B. Tanner, D.B. Romero, H. Berger, G. Margaritondo, L. Forro, Phys. Rev. B 62 (2000) 7939.
[19] L.V. Gasparov, A. Rush, G. Güntherodt, H. Berger, Phys. Rev. B 79 (2009) 144303.
[20] R. Gupta, A.K. Sood, P. Metcalf, J.M. Honig, Phys. Rev. B 65 (2002) 104430.
[21] D.M. Phase, S. Tiwari, R. Prakash, A. Dubey, V.G. Sathe, R.J. Choudhary, J. Appl. Phys. 100 (2006) 123703.
[22] J.M. Zuo, J.C.H. Spence, W. Petuskey, Phys. Rev. B 42 (1990) 8451.